A parametric study of conventional and high-speed microwave sintering of robocast porcelain

Marianna Peroglio, Christophe Meunier, Julien Favre, Jenny Faucheu, Clémence Petit

Open Ceramics 9 (2022) 100246

Contents lists available at ScienceDirect

Open Ceramics

journal homepage: www.sciencedirect.com/journal/open-ceramics

A parametric study of conventional and high-speed microwave sintering of robocast porcelain

Marianna Peroglio, Christophe Meunier, Julien Favre, Jenny Faucheu, Clémence Petit *

Mines Saint-Etienne, Université Lyon, CNRS, UMR 5307 LGF, Centre SMS, F-42023, Saint-Etienne, France

ARTICLE INFO

Keywords:
Clay 3D printer
Direct ink writing
Robocasting
Microwave hybrid heating
Porcelain

ABSTRACT

The combination of three-dimensional (3D) printing technologies and microwave (MW) sintering offers new perspectives for minimizing material, energy and time waste. This study aimed at conducting a parametric study on the sintering of robocast porcelain by conventional and MW heating in a multimode cavity (2.45 GHz, 3 kW). The effect of heating rate, dwell temperature and dwell duration on sample density, shrinkage and microstructure was investigated on small pellets. With conventional heating, a good densification was achieved with a 2 h dwell at 1250 °C, independent of heating rate (1–20 °C/min). A similar density was reached using microwave hybrid heating at a much higher heating rate (100 °C/min), shorter dwell (30 min) and slightly higher sintering temperature (1300 °C). Without susceptor, a longer pre-heating step was required to initiate the sample heating, thus extending the heat treatment duration. This study provides seeding data for the development of greener processes for aluminosilicate ceramic manufacturing.

1. Introduction

The minimization of materials, energy and time waste is the key paradigm in production processes with growing pressure due to environmental and social concerns. In the case of ceramics, this applies to all production steps, spanning the technologies used to produce the green body, the sintering process and the post-processing techniques used to obtain the final shape. Toward this aim, the association of three-dimensional (3D) printing technologies (robocasting, stereolithography) with microwave (MW) sintering is particularly interesting and has been used to produce hydroxyapatite [1,2], tricalcium phosphate [3] and alumina [4] scaffolds. On one hand, three-dimensional printing technologies help minimizing the waste of material and time, especially for the fabrication of complex shapes. On the other hand, microwave heating offers the possibility to achieve higher heating rates, reduced processing times and lower energy consumption compared to conventional heating [5–8].

Since the 1980s, different 3D printing processes have been specifically developed for ceramic manufacturing [9]. Among them, robocasting or direct ink writing is a 3D printing process where a highly loaded ceramic paste is extruded through a nozzle at ambient temperature [10]. Ceramic paste for robocasting must exhibit a shear thinning behaviour to be extruded and a sufficient yield stress to support the following layer [11]. A wide range of ceramic pastes have been developed, especially with technical ceramics such as alumina [12–14], zirconia [15,16] and calcium phosphate [17,18]. In these cases, the appropriate rheological behavior is obtained by preparing a highly loaded ceramic slurry with a controlled amount of adapted organic additives [19]. For further details, extensive reviews about recent advances in additive manufacturing of ceramics can be found here [9,20]. In comparison, 3D printing processes have been less studied concerning traditional ceramics. Of note, the adjustment of the rheological behavior can be easier for clay-based materials, such as porcelain. Porcelain starting powders contain three main components: (i) plastic raw materials (clay and kaolin), (ii) fillers (quartz) and (iii) fluxing agents (feldspar) [21,22]. When mixed with water, these powders form a paste with a certain plasticity. The rheological behavior of the paste can be adjusted by simply modifying the amount of water in the paste, without the need of organic additives [23]. Hence, a debinding step is not required, thus simplifying the firing process.

While in conventional sintering, a sample is heated by irradiation from the heating elements placed inside the oven, with microwave sintering it is possible to achieve bulk heating of the sample. As a result, in processes based on conventional heating, heat losses become increasingly important with temperature increase, while in MW based technologies there is an opposite trend since the dielectric loss tangent

* Corresponding author. .
E-mail address: clemence.petit@mines-stetienne.fr (C. Petit).

https://doi.org/10.1016/j.oceram.2022.100246
Received 17 December 2021; Received in revised form 5 March 2022; Accepted 9 March 2022
Available online 11 March 2022

increases with temperature for most materials. Hence, since several decades MW technology has been applied to a broad range of materials. In the case of ceramics it offers several advantages over conventional heating, such as a finer, more uniform microstructure, a higher densification and improved mechanical properties compared to conventional heating [24–26]. The dielectric properties of a material determine its ability to interact with microwaves and be heated [27]. Materials that possess a high dielectric loss tangent at room temperature (e.g. silicon carbide) can be readily heated at low temperatures. Conversely, materials with a low dielectric loss tangent at room temperature (e.g. alumina, porcelain) are difficult to heat at low temperatures. In this case, a microwave coupling susceptor (i.e. a material with a high dielectric loss tangent at room temperature, like silicon carbide) is added to the microwave cavity to support the sample heating [26,27]. As a result, the sample is heated both by heat irradiation from the susceptor and by microwave bulk heating of the sample itself, leading to what is referred as "hybrid microwave heating". Beside poor heating at low temperatures, another issue that is sometimes observed with microwave heating is temperature runaway (i.e. localized uncontrolled overheating of the sample), which has been observed with zirconia whose loss tangent increases with temperature [28]. The use of a susceptor helps minimizing this issue as it considerably reduces the heating gradient inside the sample (higher temperature inside the sample than on its surface) [29].

Several transformations occur during the firing process of porcelain: clay dihydroxylation (~450–600 °C), alpha-beta quartz phase transformation (~573 °C), mullite formation (>940 °C), glass formation by feldspar melting (~950–1050 °C depending on the composition), quartz dissolution (>1200 °C). These phase transformations lead to an evolution of the dielectrical properties of the material during the firing process (with an increase of tangent loss with temperature [30]), making porcelain an appealing material to investigate MW heating processes. Following sintering, mullite, quartz and a vitreous amorphous phase are formed. It is worth noting that different types of mullite can be formed: type I primary mullite, characterized by a small, low aspect ratio (<3) crystals, are found in clay relicts, and type II and type III secondary mullite, with higher aspect ratio (3–10 and > 10, respectively), found in feldspar-penetrated clay relicts [31]. Due to the complexity of porcelain composition (three main components, but also a number of minor constituents) and phase transformations, a good control of the sintering process (heating rate, dwell temperature, duration, susceptor) is particularly important to achieve optimal densification. The vitreous phase plays a critical role in the process of porcelain firing, especially in the case of very fast firing cycles. Indeed, this predominant phase controls the viscous flow sintering [32,33] and has a strong impact on the sintered porcelain final properties.

Previous studies have demonstrated the suitability of MW for fast sintering of porcelain. Already in 2007, Menezes et al. have fired sanitary, dental and electrical uniaxially-pressed porcelain in less than 35 min (excluding the cooling step) using a hybrid multimode microwave heating [34]. The final density and flexural strength of the microwave-sintered samples were comparable to the ones of samples conventionally fired in ~5 h. More recently, Lerdprom et al. observed that the viscous phase formation and sintering temperatures were lower (by > 100 °C and by ~75 °C, respectively) for porcelain sintered in a hybrid monomode microwave setup compared to conventional sintering [30]. In another study, Santos et al. have successfully fired series of relatively large objects (tableware) using an optimized hybrid microwave setup, paving the way for the scaling-up of this fast sintering process [35]. However, to the authors' best knowledge, there is up to now no parametric study on the high-speed microwave sintering of robocast porcelain. Hence, the goal of the present study was to conduct a parametric study on the sintering of robocast porcelain pellets by conventional and by microwave sintering in a multimode cavity, with and without a silicon carbide susceptor.

2. Materials and methods

An overview of the experimental design is provided in Fig. 1. Briefly, sample design was adjusted to robocast small cylinders with 100% filling. Thermal cycles were optimized to achieve maximal densification either using conventional heating (at low heating rates, up to 20 °C/min) or microwave heating (at high heating rates, up to 100 °C/min). The details of the investigated thermal cycles (heating rate, dwell temperature and duration) are reported in Table 1. The density, shrinkage behavior and microstructure of the samples were investigated.

2.1. Sample design and 3D printing

A regular commercial Limoges porcelain formulation (PT010B, Ceradel) was chosen for this study. This porcelain is already provided in plastic form (initial water content ~20 wt%), but additional deionized water was added to obtain an adequate consistency for 3D printing (final optimized water content ~24.5 wt%). A custom-made penetrometer was used to assess paste consistency and minimize batch-to-batch variations. The sample was printed using a 3D printer suitable for clay-based materials (Delta WASP 2040 clay, WASP). This 3D printing apparatus consisted of a 3D printer, an air compression system, a reservoir for the paste and a pressure regulator. The paste was introduced in the reservoir and supplied to the extruder of the 3D printer using a pressure of 4 - 5 bars.

In preliminary tests some sagging was observed. The sagging was reduced by increasing the layer height and by modifying the sample design. This involved the use of an inverted truncated cone with a 5° angle, which led to a cylinder following sagging. Printing conditions were optimized and cylinders were printed with using the following conditions: nozzle size 1.2 mm, layer height 1.2 mm, pressure 4 bars, printing speed 15 mm/s, 100% filling with a concentric pattern. Observations with an optical microscope of the printed samples validated the choice of this truncated cone design to obtain cylinders. The samples prepared by 3D printing were reproducible in size and shape. The amount of porcelain paste deposited was similar for all samples, as attested by the relatively small mass variations of the dried samples (~3% for both sample sizes).

Two sets of samples were printed: cylinders 7 mm base and 7.2 mm height for dilatometry using conventional sintering and cylinders 10 mm base and 4.8 mm height for dilatometry using microwave sintering. This difference of dimensions is related to the devices used to sinter the samples (sample holder in conventional dilatometers and sintering cells for MW sintering, see subsection 2.4 for further details). Such small samples are sometimes named "pellets" in other studies. Following robocasting, samples were dried at ambient conditions until further use. Samples were weighted and measured with a caliper after (i) printing and drying at ambient conditions, (ii) after sanding with SiC ground papers (P400, 35 μm) (when required) and (iii) after sintering.

2.2. Characterization of the powders

A robocast porcelain sample was dried and crushed using a mortar and pestle. The porcelain powder was characterized by thermogravimetric analysis and differential thermal analysis with a TGA Q50 analyser, equipped with an EGA furnace (TA Instruments) at a heating rate of 10 °C/min from room temperature to 1400 °C under a 150 mL/min nitrogen flow (after a purging step).

2.3. Conventional sintering

A series of sintering tests were carried out to find the optimal parameters to densify the samples. Based on the manufacturer's datasheet and the recent study by Ref. [36], the optimal sintering temperature was expected to be close to ~1250 °C. Hence, this temperature and a slightly above one (1300 °C) were investigated in this study. Two dwell

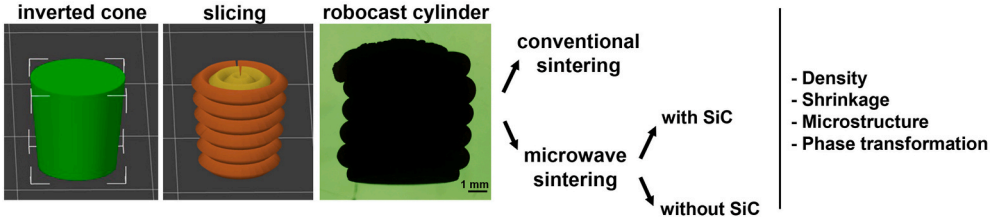

Fig. 1. Schematic view of the study design.

Table 1
Overview of the thermal cycles used to sinter robocast porcelain pellets by conventional and microwave heating (with and without SiC susceptor). The effect of heating rate, temperature and duration of the sintering dwell on the final density of robocast porcelain is reported.

Sintering type	Cycle (n.)	Heating rate (°C/min)	T dwell (°C)	t dwell (min)	Density (g/cm^3)
Conventional	1	1	1250	120	2.36
	2	5	1250	120	2.37
	3	10	1250	120	2.36
	4	20	1250	120	2.37
	5	20	1250	5	2.30
	6	20	1300	5	2.34
	7	20	1300	30	2.23
Microwave with SiC	8	20	1250	5	2.22
	9	20	1300	5	2.37
	10	50	1300	5	2.29
	11	50	1300	30	2.36
	12	100	1300	30	2.36
Microwave without SiC	13	20	1300	5	2.28
	14	50	1300	5	1.79
	15	50	1300	30	2.37

temperatures (1250 and 1300 °C), four heating rates (1, 5, 10 and 20 °C/min) and two dwell duration (5 and 120 min) were tested. Cooling was always performed at 10 °C/min.

The axial shrinkage during sintering was followed with a contact dilatometer (Setaram Setsys 16/18) (load = 5 g), equipped with a K-type thermocouple placed a few centimeters from the sample and using compressed air as carrier gas. The top surface of the samples was sanded to ensure that the two bases of the cylinder were parallel and with good contact to the displacement sensor (the opposite side of the sample did not require sanding since it was in contact with the support used for 3D printing).

2.4. Microwave sintering

Microwave sintering was conducted in a multimode parallepipedic cavity operated at 2.45 GHz and equipped with standard elements of a microwave setup. Microwaves are produced by a magnetron powered with a 3 kW generator (GMP 30KSM 56 T208 FST 3 IR, Sairem, France). A detailed description of the cavity design and its use is provided in Refs. [37,38]. The samples were placed inside a sintering cell, which was described in Ref. [38]. This cell was made of plates of thermal insulators (Rath®, which is made of insulating aluminosilicate fibers). A silicon carbide ring (outer diameter = 48 mm and inner diameter = 30 mm) was used as a susceptor and separated from the sample using a low dielectric loss ceramic tube (external diameter = 26 mm and internal diameter = 20 mm) [38]. A series of sintering tests using this sintering cell were carried out to find the optimal parameters to densify the samples. The dwell temperature was fixed at 1300 °C, and heating rates from 20 to 100 °C/min and dwell duration from 5 to 30 min were tested. The microwave generator was switched off at the end of the dwell time leading to natural cooling of the samples. Temperature was measured using a bichromatic infrared pyrometer (Lumasense Technology) placed at 40 cm from the sample. This pyrometer is sensitive to the wavelength between 2 and 2.5 μm and works in the 250–1800 °C temperature range. The emissivity ratio was set to 1. Further details about the experimental setup can be found in Refs. [38–40]. A PID feedback loop was used to control the incident power required to achieve the targeted heating rate. A Labview interface was used to record the temperature, microwave powers (incident, absorbed and reflected) and images of the sample surface. Selected cycles were also conducted without susceptor to investigate microwave/material interactions.

2.5. Characterization of the sintered samples

The density of the sintered samples was measured using the Archimedes' method with absolute ethanol. The anisotropy coefficient α was calculated on samples (with sanded lateral surface for a more precise assessment of the diameter) to allow comparison of the shrinkages in MW and conventional sintering:

$$\alpha = \frac{d_f - d_i}{d_i} \cdot \frac{h_i}{h_f - h_i}$$

where d_f and d_i stand for final and initial diameter, and h_f and h_i stand for final and initial height, respectively.

An X-ray diffractometer (X'Pert Pro MPD) with a goniometric radius of 240 mm, copper anticathode at 45 kV and 40 mA was used with a linear detector in scanning mode to perform a screening of the green bodies and sintered samples. A 2θ range from 5 to 67° with a step size of 0.02° and counting time of 250 s/step was used. PANalytical HighScore software equipped with the ICDD PDF-4+ database was used for data interpretation.

The microstructures were observed using a scanning electronic microscopy (SEM, JEOL 6500F). Before observation, samples were cut, polished down to 1 μm diamond suspension and etched for 3 min in a 5% HF solution as described by Iqbal et al. [31]. Following gold sputter coating, samples were imaged at an accelerating voltage of 20 kV with backscattered electrons to detect the different phases.

3. Results

3.1. Characterization of the porcelain powders

In the TGA-DTA analysis, a mass loss of ~0.5% was observed at ~200 °C, corresponding to the evaporation of physically-bound water. The strongest mass loss occurred between 450 and 700 °C (at 700 °C the overall mass loss was ~7.2%), which was attributed to clay dehydroxylation (i.e. transformation of kaolinite to meta-kaolinite and decomposition of chemically-bound water) (Fig. 2). This mass loss was associated with an endothermic peak at 545 °C. The mass loss was minimal at temperatures >700 °C (overall mass loss was ~7.4% at 1300 °C). An exothermic peak was observed at 990 °C, which was associated to the formation of mullite from metakaolin.

3.2. Influence of thermal cycle parameters on the final density of robocast porcelain

Final density was used as an indicator for thermal cycle optimization.

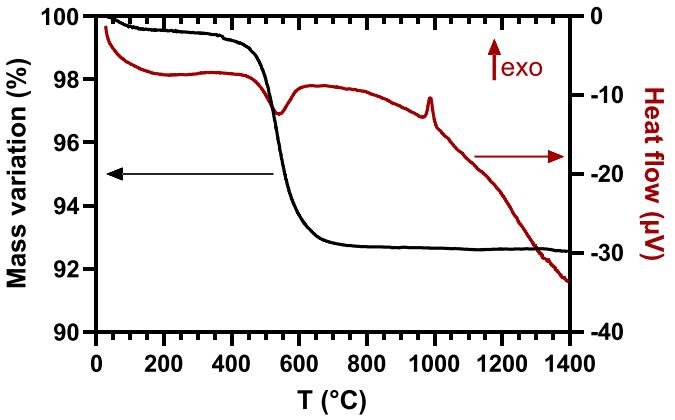

Fig. 2. Thermogravimetric (TGA) and differential thermal analysis (DTA) from 20 to 1400 °C at a scanning speed of 10 °C/min.

The effect of the thermal cycle parameters (heating rate, dwell temperature and duration, susceptor) on the final density of robocast porcelain pellets was investigated with the goal of minimizing the duration of the thermal cycle. At first, a screening at low heating rates (up to 20 °C/min) was conducted using conventional sintering. This served as a starting point for the optimization of the thermic cycle at higher heating rates (20–100 °C/min) using microwave hybrid heating. Finally, selected thermal cycles were also tested using microwave heating without SiC susceptor.

In conventional sintering, the heating rate (1–20 °C/min) did not affect the final density of the robocast porcelain samples (2.36–2.37 g/cm^3) under the chosen experimental conditions (dwell at 1250 °C for 120 min) (Table 1). As a next step, a reduction in dwell duration (from 120 to 5 min) was investigated for the highest heating rate, which led to a decrease in final density (2.30 g/cm^3). An increase in dwell temperature from 1250 to 1300 °C was not sufficient to achieve maximal density and an extension of the dwell duration at 1300 °C (from 5 to 30 min) led to a further decrease in final density (2.23 g/cm^3), suggesting that the optimal sintering conditions were surpassed. It should be noted that "overfiring" is quite common in traditional ceramics; it is typically associated to an increase of the gas pressure in closed pores, or to the reduction of Fe^{3+} impurities.

In microwave sintering with SiC susceptor, fast heating rates were explored including 20, 50 and 100 °C/min. Since it is well-known that dwell durations can be shortened using fast heating [34], a short dwell duration was chosen (5 min) and tested at 20 °C/min to allow comparison with the thermic cycles performed using conventional heating. It was found that a high densification (2.37 g/cm^3) could be achieved, but the dwell temperature had to increased to 1300 °C (Table 1). As a next step to reduce the duration of the sintering cycle, higher heating rates (50 °C and 100 °C/min) were investigated. It was found that a longer dwell time (30 instead of 5 min) was beneficial to achieve good densification (2.36 g/cm^3).

In microwave sintering without SiC, a lower density was obtained than with SiC for the thermic cycles with a short dwell duration (5 min). This was particularly evident at 50 °C/min, whereby the density obtained with and without SiC was 2.29 and 1.79 g/cm^3, respectively. Of note, increasing the dwell time from 5 to 30 min led to a good densification at 50 °C/min even without SiC.

3.3. *Influence of thermal cycle parameters on the shrinkage behavior of robocast porcelain*

In conventional heating, both the temperature corresponding to the formation of mullite and silica glass from metakaolin and the temperature corresponding to maximum densification rate increased with increasing heating rate (Fig. 3). At the lowest heating rate (1 °C/min), most of the shrinkage occurred before the beginning of the sintering dwell, while with increasing heating rate, an increasing portion of shrinkage took place during the sintering dwell (Fig. 3a). The height of the shrinkage rate peak was inversely correlated to the heating rate (Fig. 3b). The shrinkage in the x and y direction (parallel to the substrate used for 3D printing) was ~11.2%, while the shrinkage in the z direction (perpendicular to the substrate used for 3D printing) was ~16.1%. The anisotropy coefficient was 0.68 for the samples with the highest density, independent of the type of heating (conventional or MW).

In the case of high-speed (20–100 °C/min) microwave sintering with a susceptor, the metakaolin transformation temperature increased with the heating rate (Fig. 4), similarly to what has been observed at lower heating rates in conventional heating (Fig. 3). In the absence of a susceptor, the shrinkage curves appear shifted toward higher temperatures. As a result, while with SiC most of the densification occurred prior the dwell at 1300 °C, without SiC most of the densification occurred during the dwell.

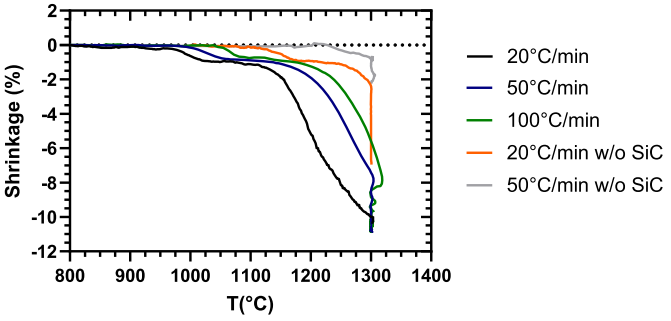

Fig. 4. Evolution of robocast porcelain pellet diameter during microwave heating with and without SiC ("w/o SiC"). The dwell duration was 30 min for all cycles, except the one at 20 °C/min for which the dwell duration was 5 min.

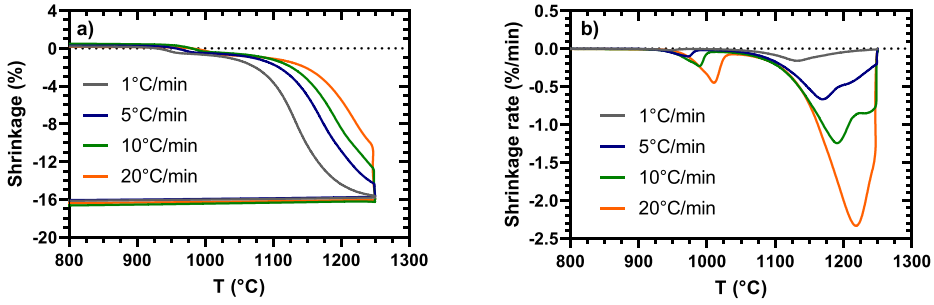

Fig. 3. Effect of the heating rate (1, 5, 10 and 20 °C/min) on the dilatometry curves obtained during conventional heating of robocast porcelain: a) shrinkage and b) shrinkage rate. Note the shift of the shrinkage curves toward higher temperatures with increasing heating rate, and the increase in magnitude and shift toward higher temperatures of the main peak in the shrinkage rate curves.

3.4. Role of the susceptor on microwave absorption by robocast porcelain

While the heating ramp (50 °C/min) could be easily followed in the presence of a susceptor, an extensive step-wise pre-heating phase was required to heat porcelain without susceptor (Fig. 5a). In fact, the targeted heating rate could only be followed from ~600 °C, which affected both the amount of incident power required (900 W versus 1450 W for the cycle with and without SiC, respectively) and the duration of the thermic cycle (from 56 to 86 min) (for a heating rate at 50 °C/min, dwell at 1300 °C for 30 min) (Fig. 5b). Of note, in the presence of SiC the incident power gradually increased with temperature increase, while without SiC the maximum incident power (that could be used without creating electric arcs, here 1450 W) was required to heat the sample until ~850 °C, after which the required incident power gradually decreased with increasing temperature (Fig. 5c). At the end of the heating ramp (at 1300 °C), the required incident power was similar with and without SiC (~1000 W).

The incident, absorbed and reflected power curves showed strong differences with and without susceptor. With susceptor, the incident and absorbed powers gradually increased with temperature and the amount of reflected power was relatively low ~300 W (Fig. 5d). Without susceptor, the incident and absorbed powers showed a marked decrease starting from ~850 °C and the reflected power was relatively high (600–700 W) (Fig. 5e). The proportion of absorbed power was higher when SiC was used (~70% with SiC and ~50% without SiC) (Fig. 5 f). The effect of an increase in material amount inside the microwave cavity on the coupling with MW was investigated by placing two samples in contact to each other. This increased the proportion of absorbed power (Fig. 5 f), but not the final density of the samples (e.g. 1.60 g/cm^3 with two samples and 1.76 g/cm^3 with one sample).

3.5. Influence of the thermal cycle on the microstructure of robocast porcelain

At low magnification, no major differences were observed in pore amount, pore size and types of phases across the selected samples (Suppl. Fig.1). At high magnification, mullite crystals of different aspect ratio were observed (Fig. 6). Following sintering at low heating rate (20 °C/min) only type I and II mullite were observed (Fig. 6a and b), while with microwave sintering at higher heating rates also type III mullite (aspect ratio >10) was observed (Fig. 6c–f). The amount of type III mullite appeared highest for samples sintered using microwave heating without susceptor (Fig. 6f).

3.6. Influence of the thermal cycle on the composition of robocast porcelain

Quartz, clay minerals (kaolinite, illite, muscovite) and microcline $KAlSi_3O_8$ were the main phases identified in the porcelain starting powders by XRD analysis (Fig. 7a and b). Following sintering, mullite, residual quartz and an amorphous glass were observed in all samples. Similar XRD diffractograms were observed for all the investigated thermal treatments.

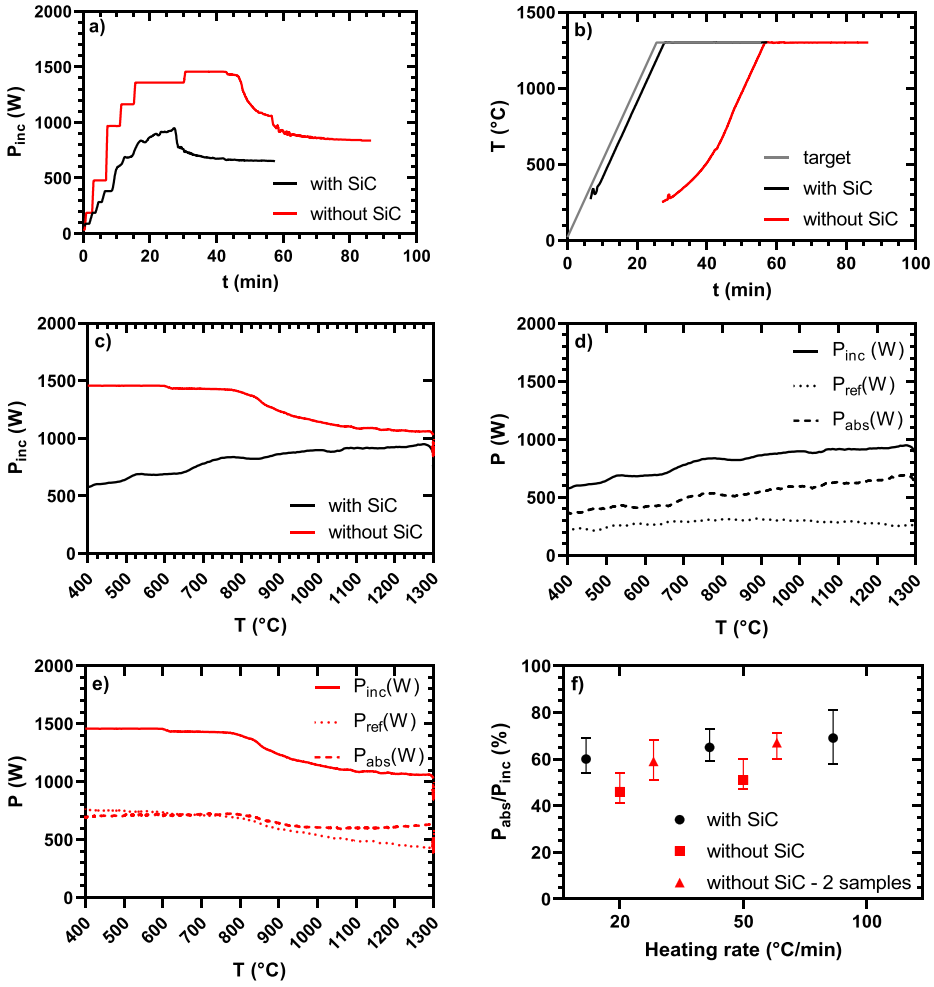

Fig. 5. Role of SiC susceptor, heating rate and sample volume on incident, absorbed and reflected powers during microwave heating of robocast porcelain. In panels a–e, data from the heating cycle at 50 °C/min with a single sample in the microwave cavity are represented. a) incident power over time, b) temperature over time, c) incident power over temperature, d) evolution of powers with SiC, e) evolution of powers without SiC, f) mean proportion of absorbed power at different heating rates with and without SiC.

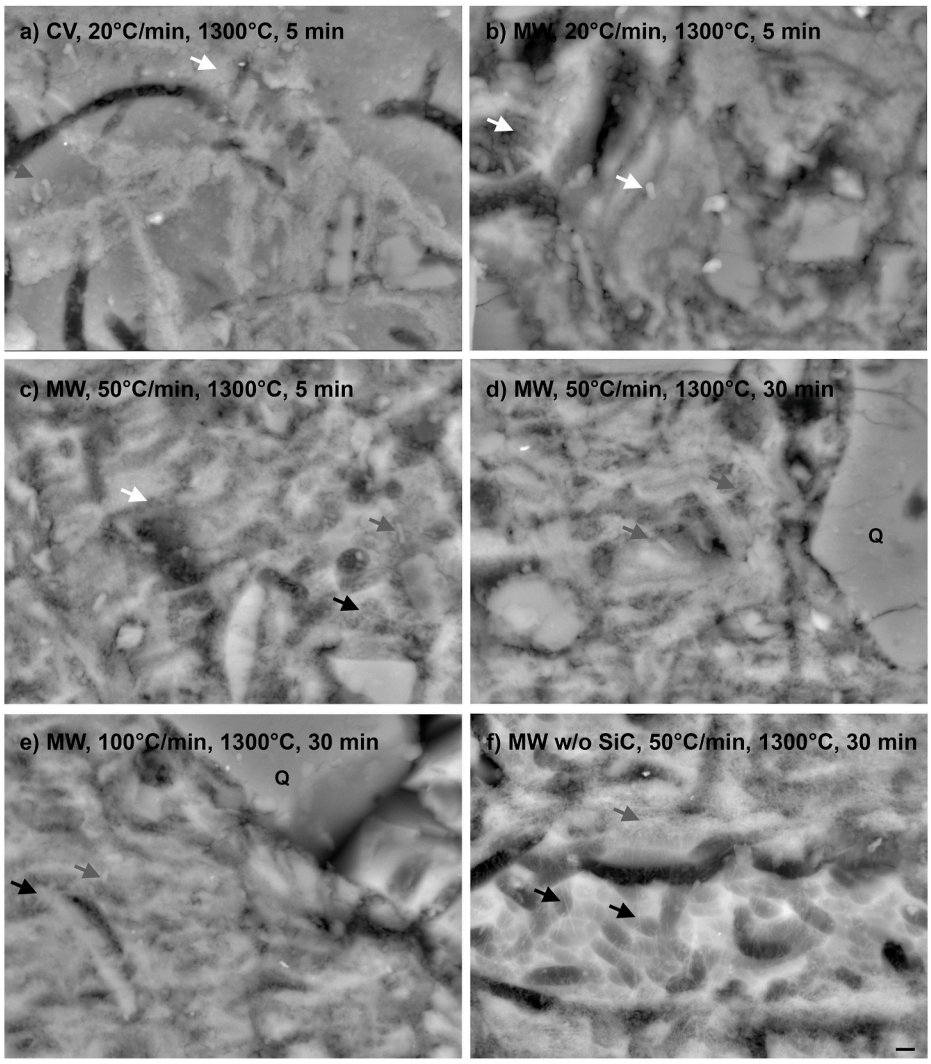

Fig. 6. High-magnification micrographs of the sintered samples using conventional (CV) and microwave (MW) sintering with and without (w/o) SiC susceptor. Different types of mullite are highlighted: white arrow for type I mullite, grey arrow for type II mullite and black arrow for type III mullite. Scale bar = 1 μm.

4. Discussion

In this study, a parametric study was conducted in order to identify optimal sintering conditions for robocast porcelain samples using MW and conventional heating.

When comparing the characteristics of the samples obtained by MW and conventional heating, similar maximal densities could be achieved with both techniques, in agreement with other studies [34]. However, it was possible to use a much higher heating rate with MW hybrid heating (100 °C/min using MW versus 20 °C/min using conventional heating). Both in conventional and MW heating, increasing the heating rate resulted in a shift of the shrinkage curves toward higher temperatures. As a result, an increasing amount of the shrinkage took place during the sintering dwell and both the metakaolin transformation temperature and the temperature corresponding to the maximum densification rate increased with increasing heating rate (Figs. 3–4 and Table 1). In conventional heating, variations in the low heating rate range (1–20 °C/min, cycles 1–4 in Table 1) had no effect on final density, possibly because the chosen conditions were already close to the optimal sintering conditions. When comparing the same thermic cycle using conventional and microwave heating, a very similar response was obtained, with a slightly lower metakaolin transformation temperature using MW (973 versus 983 °C), in line with a recent study by Santos et al. [41].

Optimal densification of porcelain results from the balance of two opposing trends taking place in the later stages of densification: sintering capillary forces and pressure from trapped gas inside the closing pores. If the optimal sintering conditions are overcome, bloating can occur, resulting in an increase of closed porosity. In agreement with the study by Manière et al. [36], bloating was observed in conventional sintering for one condition (Table 1, cycle 7).

When using MW heating without susceptor, sample heating was difficult at temperatures <600 °C due to poor material-MW coupling, in agreement with previous studies [30]. This improved starting from 600 °C (as a result of an increase in tangent loss) and from 800 °C it was possible to heat the sample at the targeted rate of 50 °C/min (Fig. 5b). The evolution of the powers vs temperature (Fig. 5e) shows a decrease of reflected power from 800 °C until the end of the thermal cycle. This can be related to an increase of loss tangent of porcelain from this temperature. Therefore, a direct MW/material interaction seems to occur from this temperature. This direct MW/material interaction is promoted once clay decomposition and removal of the chemically-bound water have been completed. However, it has to be noted that the MW experiments were carried out in a multimode cavity. In this type of cavity, the sample is surrounded by a quite high amount of materials constitutive of the sintering cell (i.e., the thermal insulators and the protective tube). The materials used inside a sintering cell are chosen for their transparency to microwaves. Nonetheless, previous authors showed that these insulating

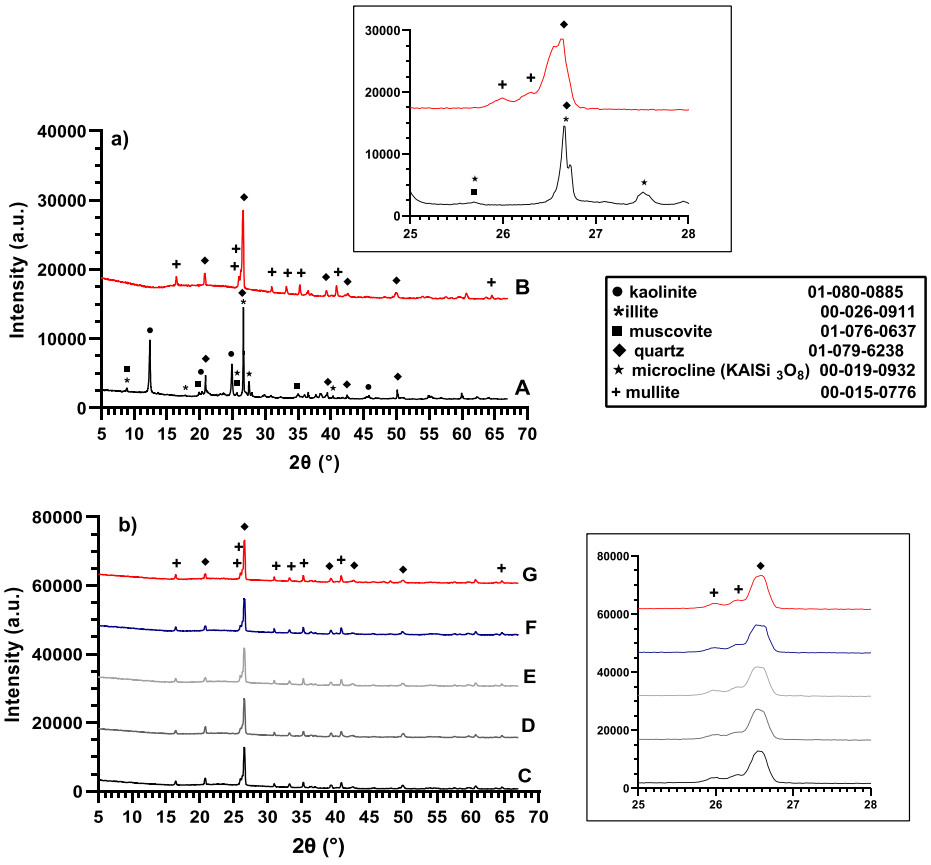

Fig. 7. X-ray diffractograms of a) porcelain green before (A) and after conventional sintering (B) and b) following different microwave thermal cycles: heating 20 °C/min, dwell 5 min (C), heating 50 °C/min, dwell 5 min (D), heating 50 °C/min, dwell 30 min (E), heating 100 °C/min, dwell 30 min (F), heating 50 °C/min, dwell 30 min (G). Cycles C–F were conducted with SiC susceptor, cycle G without SiC. In the insets, a detailed view of the 2θ = 25–28° region and references to the crystallographic datasheets used for phase identification are provided. (For interpretation of the references to colour in this figure legend, the reader is referred to the Web version of this article.)

materials can become a microwave absorbent medium and act as a susceptor [42]. Therefore, in this study the MW heating without SiC cannot be really considered as a direct MW heating. A partial indirect heating by insulating materials cannot be excluded. Even if it was possible to heat without the SiC ring, a lower final density was obtained compared to samples sintered using the same thermal cycle with susceptor. This attests the positive role of the susceptor for heat transfer for materials with low loss tangent [26]. Increasing the mass increased the proportion of absorbed power (Fig. 5f) but did not improve the final density of the samples sintered using MW heating without SiC.

No major differences were observed in the samples macrostructure (pore amount and size, phases) among the selected conditions, which is possibly due to the fact that the sintering conditions were already close to the optimum (Suppl. Fig.1). On the other hand, changes were observed in sample microstructure, i.e. the type of mullite formed was affected by the thermal cycle, in agreement with the studies by Menezes et al. and Lerdprom et al. [30,31,34]. Type I mullite was formed at low heating rates and short dwell times, while an increase in heating rate and dwell time resulted in the formation of type II and III mullite (Fig. 6). This is in agreement with the fact that crystal growth is favored by a reduction in the viscosity of the remaining viscous phase [43]. Particularly, type III mullite was predominantly observed in the samples sintered without susceptor for 30 min, for which a strong temperature gradient can be expected. In another work, Sainz et al. have investigated the evolution of crystallite and crystal size as a function of sintering temperature [44]. Based on this work, it could be expected that changes in crystallite size would precede crystal size evolution. However, further analyses are required to confirm this hypothesis.

The efficiency of microwave energy absorption depends on the dielectric properties of the material. The latter will change as its constituents undergo phase transformations during the heating ramp. In this study, the starting powders are composed of a mixture of quartz, feldspar and kaolinite. Hence, selective heating can occur even at low temperatures due to differences in the dielectric properties of these components [30]. Given the compositional heterogeneity of this material, selective heating of some of the porcelain constituents may occur, however this seems to have only a minimal impact on the overall dielectric properties of the material at temperatures below ~1000 °C. The metakaolin transformation and the formation of mullite and amorphous amorphous silica glass are associated with a dramatic change of the microwave absorption properties of the material (i.e. marked decrease in dielectric losses). Based on previous studies, a high heating rate can be kept until metakaolin transformation, but a decrease of the heating rate above this temperature is beneficial to avoid temperature runaway [34].

Measurement of the temperature in the sample core is not trivial and can lead to differences of tens or even hundreds of degrees between the measured temperature on the sample surface and the temperature in the sample core [30,45]. Therefore, special care should be taken when comparing temperatures measured using different heating methods and different tools for temperature measurement. In particular, based on the work by Santos et al. [45], the temperature of the sample core might be (i) overestimated when using a thermocouple to assess the temperature of the air inside a furnace using conventional heating, especially in the case of large samples and (ii) underestimated when using a pyrometer to assess the temperature of the sample surface when using microwave heating (especially in the setup without susceptor). It should be noted that temperature gradients between core and surface are often observed when heating samples that do not absorb microwaves well. In the case of porcelain, gradients of hundreds of degrees between the core and the surface have been reported [30]. The temperature measured by the pyrometer on the sample surface corresponds to the lowest temperature. Moreover, the temperature measurement by pyrometry is dependent on the calibration of emissivity of the pyrometers. An error in the determination of the emissivity cannot be excluded. Hence, the difference in metakaolin transformation temperature observed between conventional

and microwave sintering can be related to the difference of temperature measurement (thermocouples vs pyrometers). The difference of temperature measured by the pyrometers between MW sintering with and without SiC can be related to the temperature gradients in the sample. The temperature associated with metakaolin transformation measured on the sample surface was likely overestimated in the thermal cycles without susceptor.

The combination of 3D printing technologies with microwave sintering provides a fast method for the production of small series of samples, with minimal material waste and relatively low energy consumption for sintering. The duration of thermal treatments, and hence the production time and costs, can be strongly reduced by using microwave heating [34]. In the present study, the heating rate was increased by a factor of 5 (from 20 to 100 °C/min) when using MW hybrid heating compared to conventional heating. The dwell duration was also reduced from 120 to 30 min, but further investigations would be required to assess more precisely the reduction in dwell duration using MW.

A limitation of the present study is that while it provides an initial screening of the effect of the different parameters on the final density of robocast porcelain, a fine-tuning of the thermal cycle could be still performed (e.g. heating rate, dwell temperature and duration). Indeed, there is a general agreement that shorter dwells and sintering temperatures are required with MW sintering compared to conventional sintering [34,41,46]. This is due to the specificities of the microwave heating mode (with intensification of the electric field at interparticle contact a possible explanation) [46]. Based on the study of Menezes et al., a dwell duration of 6–10 min could be sufficient [34]. Such thermal cycle development would have a deep technological impact in terms of reduction of production costs; however, such fine-tuning goes beyond the scope of this study. Another limitation of this study is the simple geometry and small size of the samples, which was due to technical constraints (i.e. shrinkage analysis by dilatometry). Nonetheless, Santos et al. have already proven that MW heating can be successfully used to sinter series of larger objects, such as cups [35,41] and it would be interesting to test MW sintering on bigger and more complex robocast objects.

As perspectives, a further optimization of the sintering cycle with susceptor could be envisioned in order to reduce the duration of the sintering process. For instance, as described by Menezes et al. [34], a two-step heating process could be considered, with an even higher heating rate until metakaolin transformation, followed by a lower heating rate to avoid the risk of temperature runaway. It should be noted that an optimization of the reactivity of the starting powders might be needed to achieve very high heating rates. Furthermore, MW sintering could be tested on more complex robocast geometries. This may require a stricter control of the temperature gradients inside the sample during the heating phase and a finer control of the cooling phase (especially near the quartz transformation temperature).

5. Conclusions

This study provides a proof-of-concept of the suitability of MW for the sintering of robocast porcelain samples. Using MW hybrid heating it is possible to achieve high heating rates (100 °C/min) and short dwell times (5–30 min), while preserving sample final density. The duration of the thermal cycle can be strongly reduced using hybrid MW compared to CV heating (~45 min versus ~180 min, excluding the cooling step). Without a suspector, heating of porcelain in a microwave cavity is possible but challenging and requires a long heating phase at low temperatures (<600 °C). Nonetheless, a heating rate of 50 °C/min can be followed from 800 °C without a susceptor and a good densification can be obtained when ending the thermal treatment with a relatively long dwell (30 min at 1300 °C). In conventional sintering, samples were less sensitive to variations in heating rate (range: 1–20 °C/min), when a long dwell (120 min) was performed at an adequate sintering temperature (1250 °C). While no major differences were observed in the macrostructure (i.e. percentage and size of residual pores, composition of the mineral phases) of the selected sintered samples, differences in the microstructure were found, namely in the type of mullite formed. The combination of robocasting and MW sintering holds promise for quick and minimal-waste production of prototypes, small series and customized parts.

Declaration of competing interest

The authors declare that they have no known competing financial interests or personal relationships that could have appeared to influence the work reported in this paper.

Acknowledgements

This work was supported by the French Gouvernement under the Future Investments Funding Scheme of the National Research Agency (Grant number ANR-15-CRNT-000). The authors gratefully acknowledge the excellent support of Max Boudes for scanning electron microscopy, Gilles Blanc for optical microscopy, Nathalie Peillon for X-ray diffraction, Sandrine Cardinal for thermal gravimetric analysis, and Nouhaila Khalile for insightful discussions.

Appendix A. Supplementary data

Supplementary data to this article can be found online at https://doi.org/10.1016/j.oceram.2022.100246.

References

[1] Q. Wu, X. Zhang, B. Wu, W. Huang, Effects of microwave sintering on the properties of porous hydroxyapatite scaffolds, Ceram. Int. 39 (2013) 2389–2395, https://doi.org/10.1016/J.CERAMINT.2012.08.091.
[2] X. Pei, L. Ma, B. Zhang, J. Sun, Y. Sun, Y. Fan, Z. Gou, C. Zhou, X. Zhang, Creating hierarchical porosity hydroxyapatite scaffolds with osteoinduction by three-dimensional printing and microwave sintering, Biofabrication 9 (2017) 45008, https://doi.org/10.1088/1758-5090/aa90ed.
[3] S. Tarafder, V.K. Balla, N.M. Davies, A. Bandyopadhyay, S. Bose, Microwave-sintered 3D printed tricalcium phosphate scaffolds for bone tissue engineering, J. Tissue. Eng. Regenrative. Med. 7 (2013) 631–641, https://doi.org/10.1002/TERM.555.
[4] H. Curto, A. Thuault, F. Jean, M. Violier, V. Dupont, J.C. Hornez, A. Leriche, Coupling additive manufacturing and microwave sintering: a fast processing route of alumina ceramics, J. Eur. Ceram. Soc. 40 (2020) 2548–2554, https://doi.org/10.1016/J.JEURCERAMSOC.2019.11.009.
[5] R.R. Menezes, P.M. Souto, R.H.G.A. Kiminami, Microwave hybrid fast sintering of porcelain bodies, J. Mater. Process. Technol. 190 (2007) 223–229, https://doi.org/10.1016/j.jmatprotec.2007.02.041.
[6] J. Binner, K. Annapoorani, A. Paul, I. Santacruz, B. Vaidhyanathan, Dense nanostructured zirconia by two stage conventional/hybrid microwave sintering, J. Eur. Ceram. Soc. 28 (2008) 973–977, https://doi.org/10.1016/J.JEURCERAMSOC.2007.09.002.
[7] R. Taurino, A. Karamanov, R. Rosa, E. Karamanova, L. Barbieri, S. Atanasova-Vladimirova, G. Avdeev, C. Leonelli, New ceramic materials from MSWI bottom ash obtained by an innovative microwave-assisted sintering process, J. Eur. Ceram. Soc. 37 (2017) 323–331, https://doi.org/10.1016/J.JEURCERAMSOC.2016.08.011.
[8] C. Leonelli, P. Veronesi, Microwave processing of ceramic and ceramic matrix composites, in: Ceramics and Composites Processing Methods, John Wiley & Sons, Ltd, 2012, pp. 485–515, https://doi.org/10.1002/9781118176665.CH14.
[9] Z. Chen, Z. Li, J. Li, C. Liu, C. Lao, Y. Fu, C. Liu, Y. Li, P. Wang, Y. He, 3D printing of ceramics: a review, J. Eur. Ceram. Soc. 39 (2019) 661–687, https://doi.org/10.1016/J.JEURCERAMSOC.2018.11.013.
[10] J. Cesarano, A review of robocasting technology, 1. 542, MRS Online Proc. Libr. 542 (2011) 133–139, https://doi.org/10.1557/PROC-542-133, 1999.
[11] J.A. Lewis, J.E. Smay, J. Stuecker, J. Cesarano, Direct ink writing of three-dimensional ceramic structures, J. Am. Ceram. Soc. 89 (2006) 3599–3609, https://doi.org/10.1111/J.1551-2916.2006.01382.X.
[12] H.B. Denham, J.I. Cesarano, B.H. King, P. Calvert, Mechanical Behavior of Robocast Alumina, 1998, https://doi.org/10.2172/291158.
[13] T. Schlordt, F. Keppner, N. Travitzky, P. Greil, Robocasting of alumina lattice truss structures, J. Ceramic. Sci. Tech. 3 (2012) 81–88, https://doi.org/10.4416/JCST2012-00003.
[14] Z. Fu, M. Freihart, L. Wahl, T. Fey, P. Greil, N. Travitzky, Micro- and macroscopic design of alumina ceramics by robocasting, J. Eur. Ceram. Soc. 37 (2017) 3115–3124, https://doi.org/10.1016/J.JEURCERAMSOC.2017.03.052.

[15] E. Peng, X. Wei, U. Garbe, D. Yu, B. Edouard, A. Liu, J. Ding, Robocasting of dense yttria-stabilized zirconia structures, J. Mater. Sci. 53 (2018) 247–273, https://doi.org/10.1007/S10853-017-1491-X/FIGURES/11.
[16] I. Rodrigues, M. Guedes, S. Olhero, A. Chefdor, A.C. Branco, M. Leite, A.P. Serro, C. G. Figueiredo-Pina, Development of free binder zirconia-based pastes for the production of dental pieces by robocasting, J. Manuf. Process. 57 (2020) 1–9, https://doi.org/10.1016/J.JMAPRO.2020.06.015.
[17] P. Miranda, E. Saiz, K. Gryn, A.P. Tomsia, Sintering and robocasting of β-tricalcium phosphate scaffolds for orthopaedic applications, Acta Biomater. 2 (2006) 457–466, https://doi.org/10.1016/J.ACTBIO.2006.02.004.
[18] A. Lode, K. Meissner, Y. Luo, F. Sonntag, S. Glorius, B. Nies, C. Vater, F. Despang, T. Hanke, M. Gelinsky, Fabrication of porous scaffolds by three-dimensional plotting of a pasty calcium phosphate bone cement under mild conditions, J. Tissue. Eng. Regenrative. Med. 8 (2014) 682–693, https://doi.org/10.1002/TERM.1563.
[19] L. del-Mazo-Barbara, M.P. Ginebra, Rheological characterisation of ceramic inks for 3D direct ink writing: a review, J. Eur. Ceram. Soc. 41 (2021) 18–33, https://doi.org/10.1016/J.JEURCERAMSOC.2021.08.031.
[20] Y. Lakhdar, C. Tuck, J. Binner, A. Terry, R. Goodridge, Additive manufacturing of advanced ceramic materials, Prog. Mater. Sci. 116 (2021) 100736, https://doi.org/10.1016/J.PMATSCI.2020.100736.
[21] W.M. Carty, U. Senapati, Porcelain - raw materials, processing, phase evolution, and mechanical behavior, J. Am. Ceram. Soc. 81 (1998) 3–20, https://doi.org/10.1111/j.1151-2916.1998.tb02290.x.
[22] L. Carbajal, F. Rubio-Marcos, M.A. Bengochea, J.F. Fernandez, Properties related phase evolution in porcelain ceramics, J. Eur. Ceram. Soc. 27 (2007) 4065–4069, https://doi.org/10.1016/j.jeurceramsoc.2007.02.096.
[23] C.F. Revelo, H.A. Colorado, 3D printing of kaolinite clay ceramics using the Direct Ink Writing (DIW) technique, Ceram. Int. 44 (2018) 5673–5682, https://doi.org/10.1016/J.CERAMINT.2017.12.219.
[24] M. Oghbaei, O. Mirzaee, Microwave versus conventional sintering: a review of fundamentals, advantages and applications, J. Alloys Compd. 494 (2010) 175–189, https://doi.org/10.1016/j.jallcom.2010.01.068.
[25] K.I. Rybakov, E.A. Olevsky, E. v Krikun, Microwave sintering: fundamentals and modeling, J. Am. Ceram. Soc. 96 (2013) 1003–1020, https://doi.org/10.1111/JACE.12278.
[26] M. Bhattacharya, T. Basak, A review on the susceptor assisted microwave processing of materials, Energy 97 (2016) 306–338, https://doi.org/10.1016/j.energy.2015.11.034.
[27] R.R. Mishra, A.K. Sharma, Microwave-material interaction phenomena: heating mechanisms, challenges and opportunities in material processing, Compos. Appl. Sci. Manuf. 81 (2016) 78–97, https://doi.org/10.1016/j.compositesa.2015.10.035.
[28] C. Manière, T. Zahrah, E.A. Olevsky, Inherent heating instability of direct microwave sintering process: sample analysis for porous 3Y-ZrO2, Scripta Mater. 128 (2017) 49–52, https://doi.org/10.1016/J.SCRIPTAMAT.2016.10.008.
[29] C. Manière, T. Zahrah, E.A. Olevsky, Fully coupled electromagnetic-thermal-mechanical comparative simulation of direct vs hybrid microwave sintering of 3Y-ZrO2, J. Am. Ceram. Soc. 100 (2017) 2439–2450, https://doi.org/10.1111/JACE.14762.
[30] W. Lerdprom, E. Zapata-Solvas, D.D. Jayaseelan, A. Borrell, M.D. Salvador, W. E. Lee, Impact of microwave processing on porcelain microstructure, Ceram. Int. 43 (2017) 13765–13771, https://doi.org/10.1016/j.ceramint.2017.07.090.
[31] Y. Iqbal, W.E. Lee, Microstructural Evolution in Triaxial Porcelain, (n.d).
[32] C. Zanelli, M. Raimondo, G. Guarini, M. Dondi, The vitreous phase of porcelain stoneware: composition, evolution during sintering and physical properties, J. Non-Cryst. Solids 357 (2011) 3251–3260, https://doi.org/10.1016/J.JNONCRYSOL.2011.05.020.
[33] S. Conte, C. Zanelli, M. Ardit, G. Cruciani, M. Dondi, Phase evolution during reactive sintering by viscous flow: disclosing the inner workings in porcelain stoneware firing, J. Eur. Ceram. Soc. 40 (2020) 1738–1752, https://doi.org/10.1016/J.JEURCERAMSOC.2019.12.030.
[34] R.R. Menezes, P.M. Souto, R.H.G.A. Kiminami, Microwave hybrid fast sintering of porcelain bodies, J. Mater. Process. Technol. 190 (2007) 223–229, https://doi.org/10.1016/j.jmatprotec.2007.02.041.
[35] T. Santos, L.C. Costa, L. Hennetier, M.A. Valente, J. Monteiro, J. Sousa, Microwave processing of porcelain tableware using a multiple generator configuration, Appl. Therm. Eng. 50 (2013) 677–682, https://doi.org/10.1016/J.APPLTHERMALENG.2012.07.010.
[36] C. Manière, C. Harnois, S. Marinel, 3D printing of porcelain and finite element simulation of sintering affected by final stage pore gas pressure, Mater. Today Commun. 26 (2021), https://doi.org/10.1016/j.mtcomm.2021.102063.
[37] F. Zuo, C. Carry, S. Saunier, S. Marinel, D. Goeuriot, Comparison of the microwave and conventional sintering of alumina: effect of MgO doping and particle size, J. Am. Ceram. Soc. 96 (2013) 1732–1737, https://doi.org/10.1111/jace.12320.
[38] D. Zymełka, S. Saunier, J. Molimard, D. Goeuriot, Contactless monitoring of shrinkage and temperature distribution during hybrid microwave sintering, Adv. Eng. Mater. 13 (2011) 901–905, https://doi.org/10.1002/adem.201000354.
[39] J. Croquesel, D. Bouvard, J.M. Chaix, C.P. Carry, S. Saunier, Development of an instrumented and automated single mode cavity for ceramic microwave sintering: application to an alpha pure alumina powder, Mater. Des. 88 (2015) 98–105, https://doi.org/10.1016/J.MATDES.2015.08.122.
[40] F. Zuo, C. Carry, S. Saunier, S. Marinel, D. Goeuriot, Comparison of the microwave and conventional sintering of alumina: effect of MgO doping and particle size, J. Am. Ceram. Soc. 96 (2013) 1732–1737, https://doi.org/10.1111/jace.12320.
[41] T. Santos, L. Hennetier, V.A.F. Costa, L.C. Costa, Microwave versus conventional porcelain firing: colour analysis, Mater. Chem. Phys. 275 (2022), https://doi.org/10.1016/j.matchemphys.2021.125265.
[42] T. Garnault, D. Bouvard, J.M. Chaix, S. Marinel, C. Harnois, Is direct microwave heating well suited for sintering ceramics? Ceram. Int. 47 (2021) 16716–16729, https://doi.org/10.1016/J.CERAMINT.2021.02.242.
[43] J. Martín-Márquez, J.M. Rincón, M. Romero, Mullite development on firing in porcelain stoneware bodies, J. Eur. Ceram. Soc. 30 (2010) 1599–1607, https://doi.org/10.1016/J.JEURCERAMSOC.2010.01.002.
[44] M.A. Sainz, F.J. Serrano, J.M. Amigo, J. Bastida, A. Caballero, XRD microstructural analysis of mullites obtained from kaolinite–alumina mixtures, J. Eur. Ceram. Soc. 20 (2000) 403–412, https://doi.org/10.1016/S0955-2219(99)00183-1.
[45] T. Santos, L. Hennetier, V.A.F. Costa, L.C. Costa, Microwave versus conventional porcelain firing: temperature measurement, J. Manuf. Process. 41 (2019) 92–100, https://doi.org/10.1016/j.jmapro.2019.03.038.
[46] X. Qiao, X. Xie, The effect of electric field intensification at interparticle contacts in microwave sintering, 2016, Sci. Rep. 6 (2016) 1–7, https://doi.org/10.1038/srep32163, 1. 6.